Modelled connectivity of Antarctic krill spawning and nursery grounds along the Western Antarctic Peninsula

Zephyr Sylvester[1,2*], Michael S. Dinniman[3], Sally E. Thorpe[4], Kim Bernard[5†], Cassandra M. Brooks[1,2†]

[1] Department of Environmental Studies, University of Colorado Boulder, Colorado, USA 80305

[2] Institute of Arctic and Alpine Research, University of Colorado Boulder, Colorado, USA 80305

[3] Center for Coastal Physical Oceanography, Old Dominion University, Norfolk, Virginia, USA 23508

[4] British Antarctic Survey, Cambridge, CB3 0ET, United Kingdom

[5] College of Earth, Ocean, and Atmospheric Sciences, Oregon State University, Corvallis, Oregon, USA 97331

[†] These authors contributed equally to guiding this work

[*] Corresponding author: Zephyr Sylvester, email: zephyr.sylvester@colorado.edu

Keywords: Antarctic krill, connectivity, modeling, lagrangian particle tracking, transport, nursery grounds, diel vertical migration, embryo size

Abstract

Understanding the connectivity between spawning and nursery grounds of Antarctic krill (*Euphausia superba)* is essential for elucidating population dynamics and informing ecosystem-based management of krill. This study employed a regional ocean model and particle tracking to investigate larval krill transport and connectivity along the western Antarctic Peninsula (wAP), a key region for Antarctic krill, over three austral summers (2016–2019). Simulations incorporated the descent-ascent cycle of early larval development based on initial embryo sizes, along with varying larval behavior, to examine how physical and biological processes affect habitat connectivity. Results revealed that nursery ground use and retention times were closely linked to local bathymetry. Deeper regions, such as the Bransfield Strait and Marguerite Bay, retained larvae for longer durations (>50 days), while shallower nursery grounds (Gerlache Strait, Grandidier Passage) acted as secondary nursery habitats in simulations with smaller initial embryo sizes. Simulations with larger initial embryo sizes led to notable changes in retention, connectivity, and spawning locations, as more embryos successfully hatched before reaching the seafloor. Interannual wind variability emerged as a key driver of larval supply pathways, influencing connectivity between spawning areas and nursery grounds. These results highlight how a shallower hatching depth expands the range and reliability of the connectivity between spawning and nursery grounds in the wAP. By illustrating how physical forcing and biological traits jointly shape connectivity and retention between spawning and nursery grounds this study

43 emphasizes the importance of integrating biological parameterization with physical modeling
44 to better understand krill population dynamics.

45 1 Introduction

46 Antarctic krill (*Euphausia superba*, hereafter krill) are vital to the Southern Ocean
47 ecosystem, linking upper trophic levels including penguins, seals, and whales, to energy from
48 primary producers (Nicol et al. 2012, Trathan & Hill 2016, Kawaguchi et al. 2024). While
49 krill are found at a circumpolar scale, the population center is located at the northern tip of
50 the western Antarctic Peninsula (wAP) in the Southwest Atlantic (Atkinson et al. 2017,
51 Perry et al. 2019). The region is both ecologically significant supporting high levels of
52 biodiversity, as well as anthropologically significant with concentrated areas of scientific
53 research, tourism, and commercial fishing (Nicol & Foster 2016, Meyer et al. 2020). The
54 largest fishery, by biomass, in the Southern Ocean, specifically targets krill (Nicol & Foster
55 2016).
56
57 Climate-driven changes, such as warming sea temperatures (Vaughan et al. 2003, Meredith &
58 King 2005, Turner et al. 2022), shifting ocean currents and reduced sea ice coverage (Turner
59 et al. 2013, Stammerjohn et al. 2015), have been linked to declines in krill recruitment and a
60 southward shift in krill distribution in the region over the past 90 years (Atkinson et al.
61 2019). The impacts of climate change on the large and connected marine ecosystem linked
62 by advection have implications for population structure and the relative connectivity

between areas of the Antarctic. Understanding the connections between where krill are spawned and where they develop can illuminate how krill connectivity patterns may be affected by climate change.

The early life cycle of krill begins with an embryo-larvae descent-ascent cycle. After successful fertilization and spawning near the ocean surface, embryos sink to depths determined by their density relative to ambient conditions as influenced by the embryo diameter and developmental stage (Ikeda 1984, Hofmann et al. 1992). After hatching, larvae develop through several stages as they ascend back towards the surface as nauplii (Marschall & Hirche 1984). Spawning typically occurs during the austral summer (December–February, Quetin et al. 1994), though females can spawn multiple times per season under favorable food and thermal conditions (Quetin & Ross 2001, Kawaguchi 2016). Timing and frequency vary among regions and years, influenced by sea ice, food availability, and female condition (Tarling 2020).

After developing through calyptope stages, larvae become furciliae at which point they can undertake diel vertical migrations (DVM): feeding in productive surface waters at night and spending daylight hours at depth, or vice versa according to environmental conditions (Makarov 1982, Meyer et al. 2017). Despite this vertical control, early-stage krill swimming strength remains limited, rendering their horizontal movement largely passive and subject to ocean currents (Hofmann & Lascara 2000). Sea ice can further modulate larval transport by

84 providing refuge from predation and supplemental food sources (Kohlbach et al. 2017,
85 Schaafsma et al. 2017). Incorporating sea ice into models can markedly alter predicted
86 connectivity pathways relative to ocean-only simulations (Thorpe et al. 2007, Young et al.
87 2023).
88
89 The wAP is a focal region for understanding these processes, as it hosts multiple nursery
90 grounds where larval krill aggregate in early winter such as the Bransfield Strait, Gerlache
91 Strait, Grandidier Passage, and Marguerite Bay (Figure 1) (Reiss et al. 2017, Meyer et al. 2017,
92 Perry et al. 2019). Notably, the Bransfield Strait harbors greater krill abundance in winter
93 than summer, suggesting that this region is critical for overwintering (Reiss et al. 2017,
94 Meyer et al. 2017). The Gerlache Strait, meanwhile, supports overwintering *E.*
95 *crystallorophias* and adult *E. superba* (Loeb & Santora 2015), and the Grandidier Passage
96 hosts continuous bands of feeding larvae in summer with recruits concentrated on the
97 continental shelf (Perry et al. 2019). Marguerite Bay is notable for large aggregations of larval
98 krill and observations of gravid females at depth, indicating a productive spawning habitat
99 (Lascara et al. 1999, Ashjian et al. 2008). Despite this broad recognition of nursery hotspots,
100 the mechanisms linking embryonic krill transport from spawning sites to these nurseries
101 remain poorly resolved.
102
103 Changes in water mass properties and circulation along the wAP may redistribute spawning
104 grounds, influencing recruitment success (Reiss 2016, Atkinson et al. 2019). As water-mass

105 movements shift, connectivity to suitable nursery sites could be modified, potentially
106 reducing survival if krill fail to encounter suitable habitats or if sea ice coverage diminishes
107 (Meyer et al. 2017, Young et al. 2023). Resolving where embryos originate, how they move,
108 and which factors control their ultimate success is vital for both understanding krill
109 population dynamics and informing sustainable fisheries management. To address these
110 uncertainties, numerical modeling offers a powerful platform for simulating ocean–ice–krill
111 interactions at spatial and temporal resolutions difficult to achieve through field studies
112 (Johnston et al. 2022).
113
114 Here, we employ the Regional Ocean Modeling System (ROMS) configured for the Southern
115 Ocean to investigate how ocean circulation and larval behaviors, such as DVM and ice-
116 associated advection, shape connectivity pathways for early-stage krill. Our particle tracking
117 experiments integrate the embryo–larval descent–ascent cycle, capturing the transition from
118 sinking embryos to nauplii stages and culminating in the onset of DVM in the furcilia phase.
119 By focusing on the wAP, we aim to illuminate the link between spawning locations and
120 known nursery grounds, exploring how future shifts in wind, temperature, and sea ice may
121 reroute these connections. Identifying the sources and sinks of krill larvae has direct
122 relevance to fisheries and conservation policies, as decision-makers require information on
123 where to allocate resources for monitoring and what habitats merit protection under
124 dynamic environmental conditions. Through our modeling approach, we offer new insights
125 into the spatial and temporal aspects of krill larval transport, setting the stage for more

126 targeted research and management actions that support the continued productivity and
127 resilience of the Southern Ocean ecosystem.

128 2 Materials and Methods

129 2.1 Ocean Circulation Model

130 The circum-Antarctic circulation model used in this study, described by Dinniman et al.
131 (2020), is an application of ROMS, which is a primitive equation finite volume model with a
132 terrain-following vertical coordinate system (Haidvogel et al. 2008, Shchepetkin &
133 McWilliams 2009). The model includes a dynamic sea-ice model (Budgell 2005), and
134 explicitly simulates the mechanical and thermodynamic interactions between floating ice
135 shelves and the water underneath (Holland & Jenkins 1999, Dinniman et al. 2011). The
136 dynamic sea-ice model includes two-layer ice thermodynamics (Mellor & Kantha 1989,
137 Häkkinen & Mellor 1992), a snow layer, a simple estimate of frazil ice production in the
138 water column (Steele et al. 1989), and an elastic-viscous-plastic rheology (Hunke &
139 Dukowicz 1997, Hunke 2001).
140
141 The model domain includes the entire Antarctic continental shelf, including the portion
142 (~35%) of the continental shelf ocean underneath the floating ice shelves, and extends
143 northward from the continent past the annual maximum sea ice extent and across Drake
144 Passage to South America (Dinniman et al. 2020). The model grid uses a polar stereographic
145 projection with a 5-km horizontal resolution and has 32 terrain-following vertical levels

with smaller spacing near the surface and bottom. The bathymetry for the ocean and ice shelf cavities (bottom and top ocean surfaces) is from the RTopo-2 dataset (Schaffer et al. 2016), with updates in the Amundsen Sea Embayment (Millan et al. 2017).

The circum-Antarctic simulation used in this study starts after a six-year model spin-up. Lateral boundary conditions for temperature and salinity, velocity, and sea surface height are the same as in Dinniman et al. (2015, 2020). There is no need to specify sea ice boundary information as the model domain fully encompasses any sea ice observed during the satellite era (1979 to present). Following the six-year spin-up simulation, the model was run for four years using atmospheric forcing for winds, 2-m air temperatures, sea level pressure, and relative humidity obtained from the ERA5 reanalysis (Hersbach et al. 2020) covering the years 2016-2019. Precipitation and cloud fraction were specified as described in Dinniman et al. (2020) and ice shelves were assumed to be static (no thinning, thickening or iceberg calving). Characteristics of the model physical representation near Antarctica have been presented in Dinniman et al. (2020, 2023) and Galton-Fenzi et al. (2025).

2.2 Lagrangian Drifter Simulation Design

A set of online Lagrangian particle tracking simulations was conducted to incorporate unique drifter behavior across three consecutive austral summers: 2016/17, 2017/18, and 2018/19. In each simulation, one drifter was released in every 25 km by 25 km area (625 km^2) across all areas of the Antarctic continental shelf and slope, extending to a maximum seabed depth of 3,000 m, but excluding regions beneath ice shelves (Figure 1A). A total of 7,707 drifters were

167 released per deployment. Drifters were released every 14 days from November 1 through
168 March 21, resulting in 11 releases and 84,777 drifters per simulation. The release window
169 was selected to span the known timing of krill spawning across the Southern Ocean.
170 Additionally, it allows for temporal investigation of early and late season spawning events,
171 making the overall dataset more useful for other study adaptations. This approach represents
172 an idealized reality with a uniform spatial and temporal distribution of spawning. Drifters
173 were tracked until Dec. 31, 2019, with the first six months of the drifter trajectories used for
174 subsequent analyses in this study.
175
176 While this paper focuses on transport pathways between spawning and nursery grounds, the
177 full scale of the research encompasses an effort to assess the interplay between larval krill
178 behavior and interannual oceanographic variations across the entire Southern Ocean. As part
179 of that effort, additional simulations were conducted that varied drifter behavior parameters
180 such as diel vertical migration behaviors and sea ice advection rules. The alternative
181 configurations are fully described in the Supplementary Materials along with sensitivity
182 analyses of behavioral differences (see Supplementary Material). Model output from all
183 configurations are available for public download (see Data Availability).
184

185 ## 2.3 Lagrangian Drifter Configurations

186 To isolate the effects of early developmental dynamics on transport from spawning grounds,
187 we compared two simulations that were identical except for the configuration of the initial

188 embryo size assigned to each drifter (620 μm vs. 640 μm). This section outlines the shared
189 behavioral configuration used in both simulations, including: (1) temporal parameters and
190 vertical motion behaviors, (2) embryo size parameterization, (3) horizontal advection rules,
191 and (4) diel vertical migration and sea ice interactions.
192
193 Drifters were advected every model baroclinic time step (180 s) using either the three-
194 dimensional ocean velocity or the two-dimensional sea ice velocity (see below). Their
195 motion included a random vertical walk, as described by Hunter et al. (1993) and Visser
196 (1997), which was a function of the model-computed vertical turbulence. This random walk
197 was designed to represent the transport effects of parameterized vertical turbulent motions,
198 thereby enhancing the realism of drifter trajectories under varying oceanographic
199 conditions.
200
201 Vertical motions to represent early life stage behavior and DVM of krill were added to the
202 drifters. Drifters were initially released at 5 m below the surface and given an additional
203 vertical descent rate to represent the initial descent of the embryos after spawning until
204 hatching occurred at depth (Marr 1962, Quetin & Ross 1984). Drifters that reached the
205 seafloor before hatching were assumed to die (Hofmann & Hüsrevoğlu 2003, Tarling et al.
206 2007). On successful hatching, the larvae were given an additional vertical ascent rate to
207 simulate the ascent of larvae (Hofmann et al. 1992) until they reached the surface (Figure 2).
208 Vertical descent and ascent rates and hatching time were calculated off-line using the

209 embryo-larva descent-ascent model of Hofmann et al. (1992) for November–March in three
210 regions with variable water column physical properties: the Bransfield Strait, Marguerite
211 Bay, and the Bellingshausen Sea.
212
213
214
215 Embryo-larva descent-ascent rates were calculated for two different initial embryo sizes (620
216 μm and 640 μm) to span the observed range of newly released single-celled embryos (Fraser
217 1936, Marschall 1983, Quetin & Ross 1984, 2003). The average descent and ascent rates and
218 hatching times across the three locations and five months were applied to all drifters
219 according to initial embryo size (Table 1). While the average hatching time was the same
220 between initial embryo sizes, there was substantial variance in descent-ascent rates.
221 Specifically, although 620 μm embryos sank until they hatched in the off-line simulations,
222 640 μm embryos sank initially but shortly afterwards became positively buoyant and
223 ascended to the surface where they ultimately hatched. This aligns with Hofmann and
224 Hüsrevolğlu (2003), who described the positively buoyant gastrula stage for larger embryos
225 but also noted that such buoyancy does not match existing observations of early krill life
226 stages, which are not typically found at the surface (Hofmann & Hüsrevoğlu 2003 Section
227 3.4.1). Furthermore, nauplii stages have not been observed at the sea surface, implying that
228 hatching likely occurs at depth (Hempel 1979, 1985, Schnack et al. 1985). These

observations, while limited in spatial and temporal coverage, suggest that the extent to which near-surface hatching occurs remains uncertain.

Following the completion of the initial descent–ascent cycle, drifters representing newly hatched krill larvae remained near the surface and were advected horizontally by either ocean currents or sea ice drift, depending on local conditions. Drifters transitioned to sea ice advection when three criteria were met: they were located within 2 meters of the surface, more than 120 hours had elapsed since release, and the local sea ice concentration exceeded 25%. This behavioral rule was designed to reflect the tendency of larval krill to associate with sea ice when it is present, which can influence both their transport pathways and survival prospects. If these conditions were not met, drifters were advected according to ocean currents.

After 63 days, drifters were assumed to have reached a life stage capable of completing diel vertical migration (DVM) (Ikeda, 1984) and were assigned the following vertical behavior as determined dynamically based on local sea ice concentration. When sea ice concentration was below 25%, drifters followed a standard DVM pattern: they descended at 0.016 m s^{-1} during daylight hours (when the sun was above the horizon) to a maximum depth of 150m and ascended at the same rate during nighttime until reaching within 1.5m of the surface (Hudson et al. 2022) (Figure 3A). When sea ice concentration exceeded 25%, drifters switched to a reverse DVM pattern, adapted from observations of overwintering krill

250 behavior in the northwestern Weddell Sea (Meyer et al. 2017). Under this regime, drifters
251 descended at 0.016 m s^{-1} during nighttime to a maximum depth of 20m and ascended during
252 daylight hours until they were again within 1.5m of the surface (Figure 3B). This behavioral
253 switching allowed the model to capture seasonal and spatial variability in krill vertical
254 positioning in response to sea ice conditions.

255 2.4 Evaluation and Analysis

256 Spawning ground analysis along the Antarctic Peninsula was conducted by isolating the
257 starting locations of drifters that were retained within regions that represented known
258 nursery grounds. For this paper, four core nursery grounds (NG) were selected along the
259 wAP: the Bransfield Strait (BS), the Gerlache Strait (GL), the Grandidier Passage (GP), and
260 Marguerite Bay (MB) (Figure 1). Locations were selected as potential nursery grounds based
261 on prior research identifying them as hotspots for larvae and juveniles (see Introduction).
262 Each NG was defined as a fixed polygonal region using latitude and longitude bounds (shown
263 in Figure 1 and listed in Supplementary Table S1).
264
265 For each NG, 'larval influx' was identified as the number of larvae that entered an NG for
266 any duration over the simulated lifespan. 'Retention duration' was then calculated as the
267 number of days a particle remained within a specific NG. To reduce the influence of outlying
268 retention spans, the duration was reported as the median along with the interquartile range
269 (IQR), representing the middle 50% of larvae retained in each NG. Nursery ground use, or
270 'larval retention', was then determined by the retention duration within the NG. Drifters

271 were identified as retained in an NG by residing within the NG for at least 21 days within
272 their first 180 days of life. This criterion ensured that retained larvae spent three weeks of
273 larval development within a specified NG and did not merely transit through the region. The
274 'retention rate' was then expressed as the percent of larval influx retained for at least 21 days
275 after entering.
276
277 To characterize the composite spatial distribution of potential spawning locations for larvae
278 retained in each nursery, we combined the release locations across all simulation years, for
279 each embryo size. Release locations were binned into a uniform grid (0.25° latitude × 0.5°
280 longitude) and 2D histograms were computed for each nursery. Each composite histogram
281 was then normalized by the total number of retained larvae for that nursery. The normalized
282 values were then used to create maps in which each grid cell shows the percentage of that
283 nursery's retained larvae originating from that location, with all cells summing to 100. This
284 approach enables direct visual comparison of spatial distributions across nurseries.
285
286 To identify the spatial patterns of connectivity, larval trajectories of retained larvae were
287 categorized for each NG. The trajectory between spawning location and the first entrance of
288 the NG was considered the import route, while export routes were identified as the
289 trajectory after which the larvae did not re-enter the NG. For each initial embryo size, year,
290 and NG, the import and export segments were compiled across all larvae. Trajectory points
291 within the analysis region were binned into a uniform 0.25° grid to generate raw 2D

292 histograms of point density. These were then normalized by the number of contributing
293 larvae to produce maps of mean trajectory point density per larva. To facilitate visual
294 comparison across NGs, density values were scaled to percent-of-maximum and then
295 compared with year-specific animations of import and export trajectories to assess dominant
296 transport pathways. Directional summaries were produced by synthesizing dynamic patterns
297 (e.g. looping and reversals in the trajectories) not readily captured in the density maps alone.
298

299 3 Results

300 The results are presented in three parts. First, we characterize patterns of larval krill
301 retention within defined nursery grounds along the wAP (Section 3.1: Nursery Ground
302 Retention). Second, we identify the spawning locations that give rise to successful
303 recruitment in each nursery ground and describe the connectivity pathways linking them
304 (Section 3.2: Spawning Grounds and Connectivity). These first two sections are based on the
305 simulation configured with 620 µm embryos. Lastly, we assess how these patterns shift when
306 embryo size is increased to 640 µm (Section 3.3), allowing us to evaluate the influence of
307 initial embryo size on spawning locations and connectivity.

308 3.1 Nursery Ground Retention

309 The number of larvae that entered each NG (influx) varied considerably, with BS-NG
310 consistently receiving approximately three times more larvae than the other NG (Table 2,
311 embryo size 620 µm). However, retention durations were relatively consistent across the

three years simulated but showed variation between nursery grounds (Table 2). Annually, both the BS-NG and MB-NG retained 74% of larvae that passed through their boundaries. The annual median retention duration was similar in the BS and MB nursery grounds (48 and 50 days, respectively), but both nurseries showed substantial variability in duration range with IQRs exceeding 60 days (Table 2). GP-NG retained just under half of all entrants, while GS-NG had notably lower retention and the shortest median duration (Table 2). Across all nursery grounds, large IQRs indicated substantial variability in retention durations.

3.2 Spawning Grounds and Connectivity

Viable spawning locations for 620 μm embryos were restricted to areas with depths sufficient for embryos to hatch above the seafloor, typically >700 m. Of the four nursery grounds, only BS-NG and MB-NG had suitable local spawning habitats for the smaller sized embryos with 54% and 64% (respectively) of retained larvae originating locally (Table 2). Within BS-NG, much of the strait itself supported local spawning, with the southern edge of the strait contributing the highest relative share of spawning locations across all three years (Figure 4A). Spawning locations for larvae retained in BS-NG spanned a broad longitudinal range from ~80° W to nearly 50° W. In contrast, MB-NG had the most spatially restricted set of spawning locations, concentrated within deep-trough habitats of the Marguerite Trough and with no spawning occurring east of 70° W (Figure 4D).

In contrast, no local spawning occurred in GS-NG or GP-NG. Spawning locations for GS-NG overlapped substantially with those of BS-NG, with the highest relative concentrations occurring around the Boyd Strait (Figure 4B). GP-NG spawning locations also included sites within the Bransfield Strait and BS-NG, but were more diffuse along the continental shelf, with a few areas contributing higher proportions than others (Figure 4C).

Larval transport patterns from spawning locations into the GS-NG and GP-NG indicated that most larvae entered the NGs from further north except for some larvae being transported across the continental shelf and into the GP-NG (5A). While there was some interannual variability in the distribution of spawning locations, the transport pathways into both NGs remained consistent. The same was true for transport of externally spawned larvae into the MB-NG (Figure 4D). The larvae spawned off the continental shelf (Figure 4D) traveled north along the continental shelf until reaching the Marguerite Trough and were then transported into the MB-NG (Figure 5A).

The trajectories of larvae from non-local spawning locations into the BS-NG varied interannually (Figure 6A). In certain years, like the 2016–2017 and the 2017-2018 season, larvae were advected from areas along the shelf as far south as Adelaide Island along the northeastward along-slope current (Figure 5A). In the 2018–2019 season, larval transport was observed from the northwest Weddell Sea into the BS-NG.

353 Within the model, February near-surface winds over the study region also varied
354 interannually (Figure 7). During 2016–2017, strong northerlies occurred over the shelf break
355 near Boyd Strait in February (Figure 7A). In the 2018-2019 season, the wind regime shifted,
356 with weaker westerlies at the tip of the Antarctic Peninsula and a more southerly component
357 blowing northward (Figure 7C)
358
359 Despite interannual variability in spawning ground locations for the BS-NG, trajectories of
360 larvae exiting BS-NG within the 180 day-simulation remained mostly consistent across all
361 three years (Figure 6B). The primary dispersal trajectories either sent larvae north around
362 Elephant Island and toward the South Scotia Ridge, or southward through the Gerlache
363 Strait and into GS-NG and even as far as the GP-NG (Figure 5B, Figure 8A). Export of larvae
364 from the GS-NG followed the same spatial pattern, with trajectories consistently moving into
365 the GP-NG (Figure 8A) either via the Gerlache Strait or along the continental shelf and
366 around Anvers Island (Figure 5B). If larvae were exported from GP-NG, they primarily
367 moved onto the continental shelf (Figure 5B). However, in one of the three years simulated,
368 larvae were exported along the coastline of Adelaide Island (Figure 5B) and into the MB-NG
369 from the GP-NG (Figure 8A). Lastly, export of larvae from the MB-NG either exited via the
370 trough, or, more commonly, were transported further south around the tip of Alexander
371 Island (Figure 5B). Of the larvae exported out of the region, trajectories did not transport
372 larvae into any of the northern NGs (Figure 8A).
373

3.3 Embryo Size

Increasing the initial embryo size from 620 μm to 640 μm altered the patterns in larval retention, potential spawning locations, and connectivity between NGs. The number of successful spawning events was much higher and vastly increased the larval influx into all nurseries such as a nearly four-fold increase in the BS-NG and 15-fold increase in the MB-NG (Table 2). Most notably, successful spawning occurred within GS-NG and GP-NG (Table 2). These changes were accompanied by changes in retention patterns where GS-NG and GP-NG both saw median retention durations more than double (11 vs 25 days and 20 vs 44 days, respectively) thereby supporting higher retention rates (37 % vs 52 % and 46 % vs 69 %, respectively) (Table 2). In contrast, MB-NG exhibited only minor changes in retention (50 vs 58 days) and an increase in retention rate to 82% (from 74%), while BS-NG retention rates remained stable (down to 70% from 74%) and duration slightly decreased (48 days down to 41 days) (Table 2).

Spawning grounds expanded across the continental shelf in the larger embryo simulations, as evidenced by localized spawning accounting for over a quarter of retained larvae in GS-NG (26%) and GP-NG (34%) (Table 2). The spatial distribution of potential spawning locations was more diffuse with individual 0.5° grid cells rarely contributing more than 5% of a nursery's retained larvae across the wAP (Figure 9). The broader spread of potential spawning areas coincided with a decline in locally spawned larvae in BS-NG (35%) and MB-NG (34%) (Table 2), resulting in nursery populations composed of both locally derived and

395 externally supplied larvae. Despite the increase in potential spawning locations, the
396 dominant larval transport routes into each nursery remained consistent.
397
398 Connectivity between nursery grounds increased in simulations with larger embryos, with
399 both the number of inter-nursery connections and their persistence across years increasing
400 (Figure 8). This was most notable for MB-NG, where connections from GP-NG were present
401 in all three years of the 640 µm simulations (Figure 8B) compared to only one year in the 620
402 µm simulations (Figure 8A). MB-NG also received larvae from GS-NG in two of the three
403 years in the larger embryo simulations (Figure 8B). In contrast, connections from MB-NG to
404 northern nursery grounds occurred in only one of the three years (Figure 8B), and
405 connectivity between BS-NG and MB-NG did not change with embryo size (Figure 8A, B).

406 # 4 Discussion

407 ## 4.1 Nursery Use and Retention

408 Bathymetry and circulation in the wAP differentially shape simulated larval residence across
409 NGs. The assumption that embryos do not survive contact with the seafloor has ruled out
410 much of the wAP as suitable spawning habitat in prior studies (Hofmann and Hüsrevoğlu,
411 2003). While this assumption is commonly modelled (Hofmann & Hüsrevoğlu 2003, Tarling
412 et al. 2007, Thorpe et al. 2019), little empirical research on krill embryos and the seafloor has
413 been conducted. Much of the habitat within the four NGs is shallower than the ~700 m
414 needed for the simulated 620 µm embryos to hatch above the seafloor and survive (Table 1).

As a result, NGs with deeper areas, such as the BS-NG, facilitated local spawning, had higher larval influx and exhibited high retention rates and long retention durations. While the MB-NG had less influx than the BS-MB, larvae were also locally spawned and exhibited high retention rates with longer retention periods. This was likely due to a combination of the bathymetric features of the Marguerite Trough and circulation dynamics that allow larvae to remain in these regions after hatching. These results align with earlier findings that regions exceeding 1000 m in depth provide viable habitat for larval krill development (Siegel & Watkins 2016, Atkinson et al. 2019). In contrast, shallower grounds like the GS-NG and GP-NG offer briefer occupancy (<21 days) potentially due to insufficient depth for localized hatching combined with circulation patterns that promote faster export. Further analysis isolating locally hatched drifters or examining local circulation differences could clarify the drivers of these contrasting retention times.

Local spawning and prolonged residence in BS-NG and MB-NG indicate that these nurseries can support early larval development, provided sufficient food availability. In contrast, GS-NG and GP-NG did not host early larval stages but instead provided habitat for later-stage larvae advected from other areas such as BS-NG. Nursery grounds that support later stage larvae may play an important role in facilitating overwinter survival, a prerequisite for local recruitment (survival of spawned krill through their first winter, Constable 2011, Meyer et al. 2020). Our results show how physical transport and subsequent retention along the wAP

435 influence the distinct roles that different nursery grounds can play in supporting larval
436 development.
437
438 Climate trends, including warming, acidification, and declining sea ice (Flores et al. 2012,
439 Rogers et al. 2020), may alter these patterns, reducing habitat suitability in northern wAP
440 but possibly expanding southern habitats (Constable et al. 2014, Veytia et al. 2020, Sylvester
441 et al. 2021). Concurrent declines in adult body size (Atkinson et al. 2019) could lower
442 fecundity (Tarling et al. 2007, Siegel & Watkins 2016) and reshape nursery use. Nevertheless,
443 BS-NG remains relatively resilient thus far: historical hotspots have persisted despite regional
444 warming (Perry et al. 2019), suggesting that local bathymetry, circulation, and krill behavior
445 may collectively buffer some nursery grounds against broader environmental shifts.
446
447 Linking nursery use to larval survival offers valuable insights into krill recruitment
448 dynamics. Our simulations emphasize the role of seafloor depth and circulation in successful
449 embryonic and larval development, although unmodeled factors, such as prey availability,
450 predation, and variability in physiological behavior, may further shape outcomes.
451 Incorporating these drivers into models with higher spatial resolution will clarify how krill
452 populations respond to ongoing environmental change, especially in nearshore habitats that
453 are understudied, where early-stage overwintering may be crucial.

4.2 Spawning Grounds and Connectivity

In simulations using 620 µm embryos, successful spawning in the BS-NG and the MB-NG resulted in two distinct larval populations that occasionally exchanged with other nurseries, GS-NG and GP-NG, as seasonal winds and circulation modified transport paths. Interannual variability allowed some larvae from BS-NG to reach GS-NG and GP-NG as secondary nursery grounds, whereas MB-NG remained largely self-sustained and disconnected from northern areas.

Among the four nursery grounds, BS-NG displayed the most diverse spawning origins in our simulations. Across all years, a substantial portion of larvae was spawned locally, while varying wind and circulation patterns occasionally delivered additional inputs from the wAP shelf edge and the northwest Weddell Sea. These findings align with Perry et al. (2019) and the conceptual models of Conroy et al. (2020), both of which propose that localized krill productivity and wind-driven exchange shape larval distributions in slope, shelf, and coastal waters.

Transport analysis revealed how wind forcing mediates interannual variability in larval supply routes to the BS-NG. In summer 2016-2017, strong northerlies over the shelf break near Boyd Strait resulted in an anomalous (compared to the other two years) on-shelf Ekman transport that allows drifters that normally would continue to advect to the northeast in the along-slope current (Moffat & Meredith 2018) to be transported into Bransfield Strait via

Boyd Strait. By 2018–2019, the westerlies present at the tip of the Antarctic Peninsula were weaker and had a more southerly component, in agreement with previous observations by Renner et al. (2012), favoring transport from the northwest Weddell Sea instead. This demonstrates how local wind fields can either enhance or redirect larval inflows, ultimately influencing BS-NG connectivity. Despite these shifts, final dispersal routes remained consistent: export occurred north toward the South Scotia Ridge or south into GS-NG and GP-NG. MB-NG stayed relatively isolated, receiving larvae mainly from the south via the Marguerite Trough.

Future projections of strengthening and poleward-shifting westerlies under climate change (Goyal et al. 2021) suggest that wind driven circulation dynamics may undergo significant alteration to the end of the 21st century. Enhanced westerlies could reduce the frequency of southerly wind-driven transport from the Weddell Sea into BS-NG, instead favoring stronger along-slope currents that bypass Boyd Strait. Such changes could disrupt the balance of larval supply and connectivity patterns observed in this study, with implications for krill recruitment and ecosystem dynamics. Enhanced westerly-driven circulation patterns have been documented near the Antarctic Peninsula (Thompson et al. 2015, Reiss et al. 2017), where changing water-mass properties can reshape connectivity and recruitment (Atkinson et al. 2019).

As described above, the BS-NG served as a source of later-stage furcilia dispersing downstream to the GS-NG and GP-NG, often via the coastal current (Moffat et al. 2008). In GS-NG, simulated larvae had already resided in the BS-NG for at least two months indicating that they arrived as more advanced furcilia during late summer and fall. This passive transport route aligns with observed active migration routes of adult krill, which migrate inshore to the Gerlache Strait (Cleary et al. 2016) or aggregate in Bransfield Strait during winter (Reiss et al. 2017). While adult krill are capable of active migration, the overlap between active and passive routes highlights the importance of these transport corridors in maintaining connectivity between regions. In GP-NG, simulations revealed a mixing ground where larvae from BS-NG converged with those transported off-shelf from areas further south toward Marguerite Bay. This convergence highlights the role of GP-NG as a junction point for multiple transport pathways, increasing the diversity of larval origins in the nursery.

Although our circulation model is too coarse to resolve fjords and smaller-scale bathymetric features, these findings suggest that broad circulation patterns, such as the coastal current connecting BS-NG to GS-NG and GP-NG, can act as consistent larval transport routes. However, further modeling and observational studies are needed to evaluate the stability of these transport pathways and their sensitivity to environmental changes. Notably, the Gerlache Strait is a key area for winter krill fisheries (Johannessen et al. 2024). Given its ecological and economic significance, higher-resolution modeling and targeted field studies

516 are essential to better understand the interplay between larval transport, nursery ground
517 connectivity, and potential anthropogenic pressures in this region.
518
519 Under smaller embryo simulations, MB-NG remained a self-sustaining nursery. Previous
520 studies show that krill populations in Marguerite Bay exhibit complex connectivity, with
521 gravid females feeding at depth (Clarke & Tyler 2008) and high larval abundances in fall
522 along the shelf break (Ashjian et al. 2008). Piñones et al. (2013) also found that Circumpolar
523 Deep-Water intrusions maintain local populations via on-shelf spawning and remote inputs
524 from the Bellingshausen Sea. Our simulations suggest that most larvae in the MB-NG are
525 spawned locally or advected from farther south on the shelf via the Marguerite Trough, and
526 do not advect northward within their first 180 days (Figure 8). This also implies that any
527 Bellingshausen Sea connection likely involves adult or juvenile migration rather than larval
528 drift. Recent research indicates partial isolation between krill populations north and south of
529 Low Island and the southern Bransfield Strait (Gallagher et al. 2023), which may explain
530 why MB-NG acts as a mostly closed system in our simulations, reinforcing the role of
531 localized circulation in modulating connectivity.
532
533 Notably, the model omits biogeochemical processes, ocean temperature, chlorophyll-a
534 concentrations, and other ecological factors known to influence krill development and
535 habitat suitability (Ross & Quetin 1989, Piñones & Fedorov 2016) and tests a particular set of
536 behavioral assumptions. Although we account for some interannual variability in circulation

and larval transport, we do not capture the full range of processes affecting spawning success and overwintering. Future studies that incorporate wintertime surveys and additional environmental variables could refine our understanding of how circulation, behavior, and survival might be affected by changing climate conditions and productivity regimes.

4.4 Impact of Embryo Size on Spawning and Connectivity

The introduction of larger embryos in our simulations altered both the spatial distribution of successful spawning and the connectivity among nursery grounds, emphasizing the sensitivity of early-life ascent–descent cycles to poorly constrained biological parameters. Compared to smaller embryos, for which viable hatching was confined primarily to deeper habitats (e.g., the BS-NG and MB-NG) due to our assumption of seafloor mortality, larger embryos completed development in shallower waters, reducing seafloor contact and thus expanding potential spawning grounds (Hofmann et al. 1992, Capella et al. 1992).

This shift toward on-shelf hatching is consistent with earlier work suggesting that the gap between hatching depth and the ocean floor is often minimal along many parts of the wAP shelf (Hofmann & Hüsrevoğlu, 2003). Although our simulations did not incorporate seasonal changes in embryo buoyancy or descent–ascent timing (as might occur from December to March), the results raise the possibility that early-season spawning combined with larger embryo sizes could facilitate on-shelf hatching under real-world conditions. Warming temperatures may further accelerate embryonic development (Thorpe et al. 2019), suggesting that temperature-driven variability in descent–ascent cycles could be even more pronounced

than shown here. Incorporating spatially and temporally varying environmental conditions fields into future online ascent–descent models would help clarify these dynamics.

With larger embryos, overall connectivity increased among nursery grounds. GS-NG and GP-NG, previously secondary refuges used mostly by older furcilia that had drifted from BS-NG or MB-NG, became prominent nurseries supporting earlier life stages for longer periods. In some years, MB-NG, which had appeared isolated under smaller-embryo scenarios, exhibited greater inflows from GS-NG and GP-NG, reducing its apparent isolation. These findings parallel observational evidence that larval krill can occupy broad shelf regions, even while adults often aggregate nearshore in late fall (Siegel 1988, 2005, Ashjian et al. 2004). That said, we considered only seafloor-interaction mortality in these simulations. Real-world conditions likely impose additional constraints, such as predation, starvation, or physiological stress (cf. Thorpe et al. 2019), which could dampen the increased connectivity patterns observed here, especially if mortality is elevated in shallow or cold waters.

Notably, our results challenge the long-standing assumption that deep offshore spawning is the primary route for successful hatching. Early studies (Hofmann et al. 1992, Capella et al. 1992) posited that embryos contacting the seabed were non-viable, an idea reinforced by Hempel and Hempel (1986), who found deeper (>1000 m) hatching more likely based on limited sampling from seven deepwater stations. However, that limited dataset did not capture near-shelf conditions, and the paucity of comparable information from shallower

579 regions leaves open the possibility that on-shelf hatching is more common than historically
580 recognized. Expanding observational efforts, especially in on-shelf environments, could
581 either validate or refine these model outcomes.
582
583 By facilitating on-shelf spawning, larger embryos effectively blurred distinctions between
584 nearshore and oceanic habitats, intensifying cross-shelf transport and enabling more larvae
585 to reach inner-shelf areas. This outcome aligns with Piñones et al. (2013), whose model
586 simulations suggested significant on-shelf movement of shelf-break-spawned larvae, and
587 with Conroy et al. (2020), who found that spatial separation between younger and older
588 stages can be disrupted by variations in early-stage survival or behavior. If future conditions,
589 such as ongoing ocean warming, further favor on-shelf hatching, recruitment patterns along
590 the wAP may increasingly hinge on nearshore processes, influencing metapopulation
591 resilience and overall ecosystem dynamics.
592
593 Finally, we note that large uncertainties persist regarding embryo-size distributions,
594 buoyancy profiles, and stage-specific mortality rates under different environmental
595 conditions (Ross et al. 2004). Empirical data on variable sinking rates, hatching success, and
596 larval survival remain sparse, particularly in the shallow shelf zones of the wAP. Addressing
597 these gaps through laboratory experiments, long-term field campaigns, and multidisciplinary
598 collaborations will be vital to refine krill recruitment models (Johnston et al. 2022, Meyer et
599 al. 2020). By integrating more realistic representations of mortality related to temperature,

food availability, and additional sources and additional behavior strategies as necessary, future modeling efforts can better capture the full complexity of krill embryonic and larval connectivity, ultimately informing ecosystem-based management in the face of rapid environmental change.

4.5 Conclusions

Our modeling experiments indicate that bathymetry, regional circulation, and larval traits (particularly embryo size) determine connectivity between spawning areas and nursery grounds along the wAP. Interannual wind variability is a key driver of larval supply pathways, altering inflows from year to year. Embryo size influences on-shelf spawning success and connectivity among nursery regions, producing complex patterns of larval distribution, retention, and dispersal that challenge older assumptions of strictly deep-water spawning.

These findings derive from idealized models that exclude temperature-dependent mortality, acidification, and other biogeochemical factors, which may further moderate larval success. Future work integrating finer-scale hydrodynamic modeling, laboratory data on embryo buoyancy and mortality, and in situ observations, especially in poorly sampled winter or nearshore habitats, will help to further refine these mechanisms. Such efforts will enhance predictive capabilities for krill distribution in a changing climate and inform fisheries management and conservation in this ecologically and economically important region of the Southern Ocean.

Acknowledgements

Overall support for this project was provided by Pew Bertarelli Ocean Legacy. ST was funded by NERC NC-ALI funding to the British Antarctic Survey Ecosystems CONSEC Programme. ZS received additional funding from the NASA Applied Sciences, Biodiversity and Ecological Forecasting grant number 80NSSC21K1132. Simulations were performed on the Wahab High Performance Computing Cluster at Old Dominion University. Original development of the physical circulation model was supported by the US National Science Foundation under Grants ANT-1048989 and OPP-1643652 to Old Dominion University. We thank the three anonymous reviewers, whose input improved the manuscript.

Data Availability

Model output used in this study is publicly available from the Biological and Chemical Oceanography Data Management Office (BCO-DMO) and should be cited as:

Brooks CM, Dinniman M, Sylvester Z, Bernard KS, Thorpe S (2025) Modeled locations of drifters representing transport of early life stages of Antarctic krill from 2016 to 2019. https://doi.org/10.26008/1912/bco-dmo.964861.1

Literature Cited

Ashjian CJ, Davis CS, Gallager SM, Wiebe PH, Lawson GL (2008) Distribution of larval krill and zooplankton in association with hydrography in Marguerite Bay, Antarctic Peninsula, in austral fall and winter 2001 described using the Video Plankton Recorder. Deep Sea Research Part II: Topical Studies in Oceanography 55:455–471.

Ashjian CJ, Rosenwaks GA, Wiebe PH, Davis CS, Gallager SM, Copley NJ, Lawson GL, Alatalo P (2004) Distribution of zooplankton on the continental shelf off Marguerite Bay, Antarctic Peninsula, during Austral Fall and Winter, 2001. Deep Sea Research Part II: Topical Studies in Oceanography 51:2073–2098.

Atkinson A, Hill SL, Pakhomov EA, Siegel V, Anadon R, Chiba S, Daly KL, Downie R, Fielding S, Fretwell P, Gerrish L, Hosie GW, Jessopp MJ, Kawaguchi S, Krafft BA, Loeb V, Nishikawa J, Peat HJ, Reiss CS, Ross RM, Quetin LB, Schmidt K, Steinberg

DK, Subramaniam RC, Tarling GA, Ward P (2017) KRILLBASE: a circumpolar database of Antarctic krill and salp numerical densities, 1926–2016. Earth System Science Data 9:193–210.

Atkinson A, Hill SL, Pakhomov EA, Siegel V, Reiss CS, Loeb VJ, Steinberg DK, Schmidt K, Tarling GA, Gerrish L, Sailley SF (2019) Krill (Euphausia superba) distribution contracts southward during rapid regional warming. Nature Clim Change 9:142–147.

Budgell WP (2005) Numerical simulation of ice-ocean variability in the Barents Sea region. Ocean Dynamics 55:370–387.

Capella JE, Quetin LB, Hofmann EE, Ross RM (1992) Models of the early life history of Euphausia superba—Part II. Lagrangian calculations. Deep Sea Research Part A Oceanographic Research Papers 39:1201–1220.

Clarke A, Tyler PA (2008) Adult Antarctic Krill Feeding at Abyssal Depths. Current Biology 18:282–285.

Cleary A, Durbin E, Casas M, Zhou M (2016) Winter distribution and size structure of Antarctic krill Euphausia superba populations in-shore along the West Antarctic Peninsula. Mar Ecol Prog Ser 552:115–129.

Conroy JA, Reiss CS, Gleiber MR, Steinberg DK (2020) Linking Antarctic krill larval supply and recruitment along the Antarctic Peninsula. Integrative and Comparative Biology 60:1386–1400.

Constable AJ (2011) Lessons from CCAMLR on the implementation of the ecosystem approach to managing fisheries: Lessons from CCAMLR on EBFM. Fish and Fisheries 12:138–151.

Constable AJ, Melbourne-Thomas J, Corney SP, Arrigo KR, Barbraud C, Barnes DKA, Bindoff NL, Boyd PW, Brandt A, Costa DP, Davidson AT, Ducklow HW, Emmerson L, Fukuchi M, Gutt J, Hindell MA, Hofmann EE, Hosie GW, Iida T, Jacob S, Johnston NM, Kawaguchi S, Kokubun N, Koubbi P, Lea M-A, Makhado A, Massom RA, Meiners K, Meredith MP, Murphy EJ, Nicol S, Reid K, Richerson K, Riddle MJ, Rintoul SR, Smith WO, Southwell C, Stark JS, Sumner M, Swadling KM, Takahashi KT, Trathan PN, Welsford DC, Weimerskirch H, Westwood KJ, Wienecke BC, Wolf-Gladrow D, Wright SW, Xavier JC, Ziegler P (2014) Climate change and Southern Ocean ecosystems I: how changes in physical habitats directly affect marine biota. Global Change Biology 20:3004–3025.

Dinniman MS, Klinck JM, Bai L-S, Bromwich DH, Hines KM, Holland DM (2015) The Effect of Atmospheric Forcing Resolution on Delivery of Ocean Heat to the Antarctic Floating Ice Shelves. Journal of Climate 28:6067–6085.

Dinniman MS, Klinck JM, Smith WO (2011) A model study of Circumpolar Deep Water on the West Antarctic Peninsula and Ross Sea continental shelves. Deep Sea Research Part II: Topical Studies in Oceanography 58:1508–1523.

Dinniman MS, St-Laurent P, Arrigo KR, Hofmann EE, van Dijken GL (2020) Analysis of Iron Sources in Antarctic Continental Shelf Waters. Journal of Geophysical Research: Oceans 125:e2019JC015736.

690 Dinniman MS, St-Laurent P, Arrigo KR, Hofmann EE, van Dijken GL (2023) Sensitivity of
691 the Relationship Between Antarctic Ice Shelves and Iron Supply to Projected Changes
692 in the Atmospheric Forcing. Journal of Geophysical Research: Oceans
693 128:e2022JC019210.
694 Flores H, Atkinson A, Kawaguchi S, Krafft B, Milinevsky G, Nicol S, Reiss C, Tarling G,
695 Werner R, Bravo Rebolledo E, Cirelli V, Cuzin-Roudy J, Fielding S, van Franeker J,
696 Groeneveld J, Haraldsson M, Lombana A, Marschoff E, Meyer B, Pakhomov E, Van de
697 Putte A, Rombolá E, Schmidt K, Siegel V, Teschke M, Tonkes H, Toullec J, Trathan P,
698 Tremblay N, Werner T (2012) Impact of climate change on Antarctic krill. Mar Ecol
699 Prog Ser 458:1–19.
700 Fraser FC (Francis C (1936) On the development and distribution of the young stages of Krill
701 (Euphausia superba). Discovery reports 14:1–192.
702 Gallagher KL, Dinniman MS, Lynch HJ (2023) Quantifying Antarctic krill connectivity
703 across the West Antarctic Peninsula and its role in large-scale Pygoscelis penguin
704 population dynamics. Sci Rep 13:12072.
705 Galton-Fenzi BK, Porter-Smith R, Cook S, Cougnon E, Gwyther DE, Huneke WGC,
706 Rosevear MG, Asay-Davis X, Boeira Dias F, Dinniman MS, Holland D, Kusahara K,
707 Naughten KA, Nicholls KW, Pelletier C, Richter O, Seroussi HL, Timmermann R
708 (2025) Realistic ice-shelf/ocean state estimates (RISE) of Antarctic basal melting and
709 drivers. EGUsphere:1–27.
710 Goyal R, Gupta AS, Jucker M, England MH (2021) Historical and Projected Changes in the
711 Southern Hemisphere Surface Westerlies. Geophysical Research Letters
712 48:e2020GL090849.
713 Haidvogel DB, Arango H, Budgell WP, Cornuelle BD, Curchitser E, Di Lorenzo E, Fennel K,
714 Geyer WR, Hermann AJ, Lanerolle L, Levin J, McWilliams JC, Miller AJ, Moore AM,
715 Powell TM, Shchepetkin AF, Sherwood CR, Signell RP, Warner JC, Wilkin J (2008)
716 Ocean forecasting in terrain-following coordinates: Formulation and skill assessment
717 of the Regional Ocean Modeling System. Journal of Computational Physics 227:3595–
718 3624.
719 Häkkinen S, Mellor GL (1992) Modeling the seasonal variability of a coupled Arctic ice-
720 ocean system. J Geophys Res 97:20285.
721 Hempel I (1979) Vertical distribution of eggs and nauplii of krill (Euphausia superba) south
722 of Elephant Island. Meeresforschung 27:119–123.
723 Hempel I (1985) Vertical Distribution of Larvae of Antarctic Krill, Euphausia superba. In:
724 *Antarctic Nutrient Cycles and Food Webs*. Siegfried WR, Condy PR, Laws RM (eds)
725 Springer Berlin Heidelberg, Berlin, Heidelberg, p 308–310
726 Hempel I, Hempel G (1986) Field observations on the developmental ascent of larval
727 Euphausia superba (Crustacea). Polar Biol 6:121–126.
728 Hersbach H, Bell B, Berrisford P, Hirahara S, Horányi A, Muñoz-Sabater J, Nicolas J, Peubey
729 C, Radu R, Schepers D, Simmons A, Soci C, Abdalla S, Abellan X, Balsamo G,
730 Bechtold P, Biavati G, Bidlot J, Bonavita M, Chiara G, Dahlgren P, Dee D,

731 Diamantakis M, Dragani R, Flemming J, Forbes R, Fuentes M, Geer A, Haimberger L,
732 Healy S, Hogan RJ, Hólm E, Janisková M, Keeley S, Laloyaux P, Lopez P, Lupu C,
733 Radnoti G, Rosnay P, Rozum I, Vamborg F, Villaume S, Thépaut J (2020) The ERA5
734 global reanalysis. QJR Meteorol Soc 146:1999–2049.
735 Hofmann E, Capella JE, Ross RM, Quetin LB (1992) Models of the early life history of
736 Euphausia superba—Part I. Time and temperature dependence during the descent-
737 ascent cycle. Deep Sea Research Part A Oceanographic Research Papers 39:1177–
738 1200.
739 Hofmann E, Hüsrevoğlu Y (2003) A circumpolar modeling study of habitat control of
740 Antarctic krill (Euphausia superba) reproductive success. Deep Sea Research Part II:
741 Topical Studies in Oceanography 50:3121–3142.
742 Hofmann E, Lascara C (2000) Modeling the growth dynamics of Antarctic krill Euphausia
743 superba. Mar Ecol Prog Ser 194:219–231.
744 Holland DM, Jenkins A (1999) Modeling Thermodynamic Ice–Ocean Interactions at the Base
745 of an Ice Shelf. Journal of Physical Oceanography 29:1787–1800.
746 Hudson K, Oliver MJ, Kohut J, Cohen JH, Dinniman MS, Klinck JM, Reiss CS, Cutter GR,
747 Statscewich H, Bernard KS, Fraser W (2022) Subsurface Eddy Facilitates Retention of
748 Simulated Diel Vertical Migrators in a Biological Hotspot. JGR Oceans 127.
749 Hunke EC (2001) Viscous–Plastic Sea Ice Dynamics with the EVP Model: Linearization
750 Issues. Journal of Computational Physics 170:18–38.
751 Hunke EC, Dukowicz JK (1997) An Elastic–Viscous–Plastic Model for Sea Ice Dynamics.
752 Journal of Physical Oceanography 27:1849–1867.
753 Hunter JR, Craig PD, Phillips HE (1993) On the use of random walk models with spatially
754 variable diffusivity. Journal of Computational Physics 106:366–376.
755 Ikeda T (1984) Development of the larvae of the Antarctic krill (Euphausia superba Dana)
756 observed in the laboratory. Journal of Experimental Marine Biology and Ecology
757 75:107–117.
758 Johannessen ED, Krafft BA, Donovan CR, Wiff R, Caneco B, Lowther A (2024) Sensitivity of
759 the stock assessment for the Antarctic krill fishery to time-varying natural and fishing
760 mortality. Fisheries Management and Ecology 31:e12721.
761 Johnston NM, Murphy EJ, Atkinson A, Constable AJ, Cotté C, Cox M, Daly KL, Driscoll R,
762 Flores H, Halfter S, Henschke N, Hill SL, Höfer J, Hunt BPV, Kawaguchi S, Lindsay D,
763 Liszka C, Loeb V, Manno C, Meyer B, Pakhomov EA, Pinkerton MH, Reiss CS,
764 Richerson K, Jr. WOS, Steinberg DK, Swadling KM, Tarling GA, Thorpe SE, Veytia D,
765 Ward P, Weldrick CK, Yang G (2022) Status, Change, and Futures of Zooplankton in
766 the Southern Ocean. Frontiers in Ecology and Evolution 9.
767 Kawaguchi S (2016) Reproduction and Larval Development in Antarctic Krill (Euphausia
768 superba). In: *Biology and Ecology of Antarctic Krill*. Advances in Polar Ecology,
769 Siegel V (ed) Springer International Publishing, Cham, p 225–246

Kawaguchi S, Atkinson A, Bahlburg D, Bernard KS, Cavan EL, Cox MJ, Hill SL, Meyer B, Veytia D (2024) Climate change impacts on Antarctic krill behaviour and population dynamics. Nat Rev Earth Environ 5:43–58.

Kohlbach D, Lange BA, Schaafsma FL, David C, Vortkamp M, Graeve M, van Franeker JA, Krumpen T, Flores H (2017) Ice Algae-Produced Carbon Is Critical for Overwintering of Antarctic Krill Euphausia superba. Front Mar Sci 4.

Lascara CM, Hofmann EE, Ross RM, Quetin LB (1999) Seasonal variability in the distribution of Antarctic krill, Euphausia superba, west of the Antarctic Peninsula. Deep Sea Research Part I: Oceanographic Research Papers 46:951–984.

Loeb VJ, Santora JA (2015) Climate variability and spatiotemporal dynamics of five Southern Ocean krill species. Progress in Oceanography 134:93–122.

Makarov RR (1982) Ontogenetic migrations in Antarctic euphausiids: “The Antarctic”.

Marr J (1962) The Natural History and Geography of the Antarctic Krill (Euphausia superba Dana). Discovery Reports32, pp. 33–464. Cambridge: University Press 1962. 10, – £. Int Revue ges Hydrobiol Hydrogr 32:33–637.

Marschall HP (1983) Sinking speed, density and size of Euphausiid eggs. Meeresforsch 30:1–9.

Marschall H-P, Hirche H-J (1984) Development of eggs and nauplii of Euphausia superba. Polar Biol 2:245–250.

Mellor GL, Kantha L (1989) An ice-ocean coupled model. Journal of Geophysical Research: Oceans 94:10937–10954.

Meredith MP, King JC (2005) Rapid climate change in the ocean west of the Antarctic Peninsula during the second half of the 20th century: RAPID OCEAN CLIMATE CHANGE AT THE WAP. Geophys Res Lett 32:n/a-n/a.

Meyer B, Atkinson A, Bernard KS, Brierley AS, Driscoll R, Hill SL, Marschoff E, Maschette D, Perry FA, Reiss CS, Rombolá E, Tarling GA, Thorpe SE, Trathan PN, Zhu G, Kawaguchi S (2020) Successful ecosystem-based management of Antarctic krill should address uncertainties in krill recruitment, behaviour and ecological adaptation. Communications Earth & Environment 1:1–12.

Meyer B, Freier U, Grimm V, Groeneveld J, Hunt BPV, Kerwath S, King R, Klaas C, Pakhomov E, Meiners KM, Melbourne-Thomas J, Murphy EJ, Thorpe SE, Stammerjohn S, Wolf-Gladrow D, Auerswald L, Götz A, Halbach L, Jarman S, Kawaguchi S, Krumpen T, Nehrke G, Ricker R, Sumner M, Teschke M, Trebilco R, Yilmaz NI (2017) The winter pack-ice zone provides a sheltered but food-poor habitat for larval Antarctic krill. Nature Ecology & Evolution 1:1853–1861.

Millan R, Rignot E, Bernier V, Morlighem M, Dutrieux P (2017) Bathymetry of the Amundsen Sea Embayment sector of West Antarctica from Operation IceBridge gravity and other data. Geophys Res Lett 44:1360–1368.

Moffat C, Beardsley RC, Owens B, van Lipzig N (2008) A first description of the Antarctic Peninsula Coastal Current. Deep Sea Research Part II: Topical Studies in Oceanography 55:277–293.

811 Moffat C, Meredith M (2018) Shelf–ocean exchange and hydrography west of the Antarctic
812 Peninsula: a review. Philosophical Transactions of the Royal Society A: Mathematical,
813 Physical and Engineering Sciences 376:20170164.
814 Nicol S, Foster J (2016) The Fishery for Antarctic Krill: Its Current Status and Management
815 Regime. In: *Biology and Ecology of Antarctic Krill*. Advances in Polar Ecology, Siegel
816 V (ed) Springer International Publishing, Cham, p 387–421
817 Nicol S, Foster J, Kawaguchi S (2012) The fishery for Antarctic krill - recent developments:
818 Krill fishery review. Fish and Fisheries 13:30–40.
819 Perry FA, Atkinson A, Sailley SF, Tarling GA, Hill SL, Lucas CH, Mayor DJ (2019) Habitat
820 partitioning in Antarctic krill: Spawning hotspots and nursery areas. PLOS ONE
821 14:e0219325.
822 Piñones A, Fedorov AV (2016) Projected changes of Antarctic krill habitat by the end of the
823 21st century: Changes in Antarctic Krill Habitat. Geophysical Research Letters
824 43:8580–8589.
825 Piñones A, Hofmann E, Daly K, Dinniman M, Klinck J (2013) Modeling the remote and local
826 connectivity of Antarctic krill populations along the western Antarctic Peninsula.
827 Mar Ecol Prog Ser 481:69–92.
828 Quetin LB, Ross RM (1984) Depth distribution of developing Euphausia superba embryos,
829 predicted from sinking rates. Mar Biol 79:47–53.
830 Quetin LB, Ross RM (2001) Environmental Variability and Its Impact on the Reproductive
831 Cycle of Antarctic Krill. Am Zool 41:74–89.
832 Quetin LB, Ross RM (2003) Episodic recruitment in Antarctic krill Euphausia superba in the
833 Palmer LTER study region. Mar Ecol Prog Ser 259:185–200.
834 Quetin LB, Ross RM, Clarke A (1994) Krill energetics: seasonal and environmental aspects of
835 the physiology of Euphausia superba.
836 Reiss CS (2016) Age, Growth, Mortality, and Recruitment of Antarctic Krill, Euphausia
837 superba. In: *Biology and Ecology of Antarctic Krill*. Advances in Polar Ecology, Siegel
838 V (ed) Springer International Publishing, Cham, p 101–144
839 Reiss CS, Cossio A, Santora JA, Dietrich KS, Murray A, Mitchell BG, Walsh J, Weiss EL,
840 Gimpel C, Jones CD, Watters GM (2017) Overwinter habitat selection by Antarctic
841 krill under varying sea-ice conditions: implications for top predators and fishery
842 management. Marine Ecology Progress Series 568:1–16.
843 Renner AHH, Thorpe SE, Heywood KJ, Murphy EJ, Watkins JL, Meredith MP (2012)
844 Advective pathways near the tip of the Antarctic Peninsula: Trends, variability and
845 ecosystem implications. Deep Sea Research Part I: Oceanographic Research Papers
846 63:91–101.
847 Rogers AD, Frinault BAV, Barnes DKA, Bindoff NL, Downie R, Ducklow HW, Friedlaender
848 AS, Hart T, Hill SL, Hofmann EE, Linse K, McMahon CR, Murphy EJ, Pakhomov EA,
849 Reygondeau G, Staniland IJ, Wolf-Gladrow DA, Wright R (2020) Antarctic Futures:
850 An Assessment of Climate-Driven Changes in Ecosystem Structure, Function, and

Service Provisioning in the Southern Ocean. Annual Review of Marine Science 12:null.

Ross RM, Quetin LB (1989) Energetic cost to develop to the first feeding stage of *Euphausia superba* Dana and the effect of delays in food availability. Journal of Experimental Marine Biology and Ecology 133:103–127.

Ross RM, Quetin LB, Newberger T, Oakes SA (2004) Growth and behavior of larval krill (*Euphausia superba*) under the ice in late winter 2001 west of the Antarctic Peninsula. Deep Sea Research Part II: Topical Studies in Oceanography 51:2169–2184.

Schaafsma FL, Kohlbach D, David C, Lange BA, Graeve M, Flores H, Franeker JA van (2017) Spatio-temporal variability in the winter diet of larval and juvenile Antarctic krill, *Euphausia superba*, in ice-covered waters. Marine Ecology Progress Series 580:101–115.

Schaffer J, Timmermann R, Arndt JE, Kristensen SS, Mayer C, Morlighem M, Steinhage D (2016) A global, high-resolution data set of ice sheet topography, cavity geometry, and ocean bathymetry. Earth Syst Sci Data 8:543–557.

Schnack SB, Marschall S, Mizdalski E (1985) On the distribution of copepods and larvae of Euphausia superba in Antarctic waters during February 1982. Meeresforschung 30:251–263.

Shchepetkin AF, McWilliams JC (2009) Correction and commentary for "Ocean forecasting in terrain-following coordinates: Formulation and skill assessment of the regional ocean modeling system" by Haidvogel et al., J. Comp. Phys. 227, pp. 3595–3624. Journal of Computational Physics 228:8985–9000.

Siegel V (1988) A Concept of Seasonal Variation of Krill (Euphausia superba) Distribution and Abundance West of the Antarctic Peninsula. In: *Antarctic Ocean and Resources Variability*. Sahrhage D (ed) Springer Berlin Heidelberg, Berlin, Heidelberg, p 219–230

Siegel V (2005) Distribution and population dynamics of Euphausia superba: summary of recent findings. Polar Biol 29:1–22.

Siegel V, Watkins JL (2016) Distribution, Biomass and Demography of Antarctic Krill, Euphausia superba. In: *Biology and Ecology of Antarctic Krill*. Advances in Polar Ecology, Siegel V (ed) Springer International Publishing, Cham, p 21–100

Stammerjohn SE, Maksym T, Massom RA, Lowry KE, Arrigo KR, Yuan X, Raphael M, Randall-Goodwin E, Sherrell RM, Yager PL (2015) Seasonal sea ice changes in the Amundsen Sea, Antarctica, over the period of 1979–2014. Elementa: Science of the Anthropocene 3:000055.

Steele M, Mellor GL, Mcphee MG (1989) Role of the Molecular Sublayer in the Melting or Freezing of Sea Ice. J Phys Oceanogr 19:139–147.

Sylvester ZT, Long MC, Brooks CM (2021) Detecting Climate Signals in Southern Ocean Krill Growth Habitat. Front Mar Sci 0.

Tarling GA (2020) Routine metabolism of Antarctic krill (Euphausia superba) in South Georgia waters: absence of metabolic compensation at its range edge. Mar Biol 167:108.

Tarling GA, Cuzin-Roudy J, Thorpe SE, Shreeve RS, Ward P, Murphy EJ (2007) Recruitment of Antarctic krill Euphausia superba in the South Georgia region: adult fecundity and the fate of larvae. Marine Ecology Progress Series 331:161–179.

Thompson DWJ, Barnes EA, Deser C, Foust WE, Phillips AS (2015) Quantifying the Role of Internal Climate Variability in Future Climate Trends. Journal of Climate 28:6443–6456.

Thorpe S, Tarling G, Murphy E (2019) Circumpolar patterns in Antarctic krill larval recruitment: an environmentally driven model. Marine Ecology Progress Series 613:77–96.

Thorpe SE, Murphy EJ, Watkins JL (2007) Circumpolar connections between Antarctic krill (Euphausia superba Dana) populations: Investigating the roles of ocean and sea ice transport. Deep Sea Research Part I: Oceanographic Research Papers 54:792–810.

Trathan PN, Hill SL (2016) The Importance of Krill Predation in the Southern Ocean. In: *Biology and Ecology of Antarctic Krill*. Advances in Polar Ecology, Siegel V (ed) Springer International Publishing, Cham, p 321–350

Turner J, Holmes C, Caton Harrison T, Phillips T, Jena B, Reeves-Francois T, Fogt R, Thomas ER, Bajish CC (2022) Record Low Antarctic Sea Ice Cover in February 2022. Geophysical Research Letters 49:e2022GL098904.

Turner J, Maksym T, Phillips T, Marshall GJ, Meredith MP (2013) The impact of changes in sea ice advance on the large winter warming on the western Antarctic Peninsula. Int J Climatol 33:852–861.

Vaughan DG, Marshall GJ, Connolley WM, Parkinson C, Mulvaney R, Hodgson DA, King JC, Pudsey CJ, Turner J (2003) Recent rapid regional climate warming on the Antarctic Peninsula. Climatic Change 60:243–274.

Veytia D, Corney S, Meiners KM, Kawaguchi S, Murphy EJ, Bestley S (2020) Circumpolar projections of Antarctic krill growth potential. Nature Climate Change:1–8.

Visser A (1997) Using random walk models to simulate the vertical distribution of particles in a turbulent water column. Mar Ecol Prog Ser 158:275–281.

Young EF, Thorpe SE, Renner AHH, Murphy EJ (2023) Environmental and behavioural drivers of Antarctic krill distribution at the South Orkney Islands: A regional perspective. Journal of Marine Systems:103920.

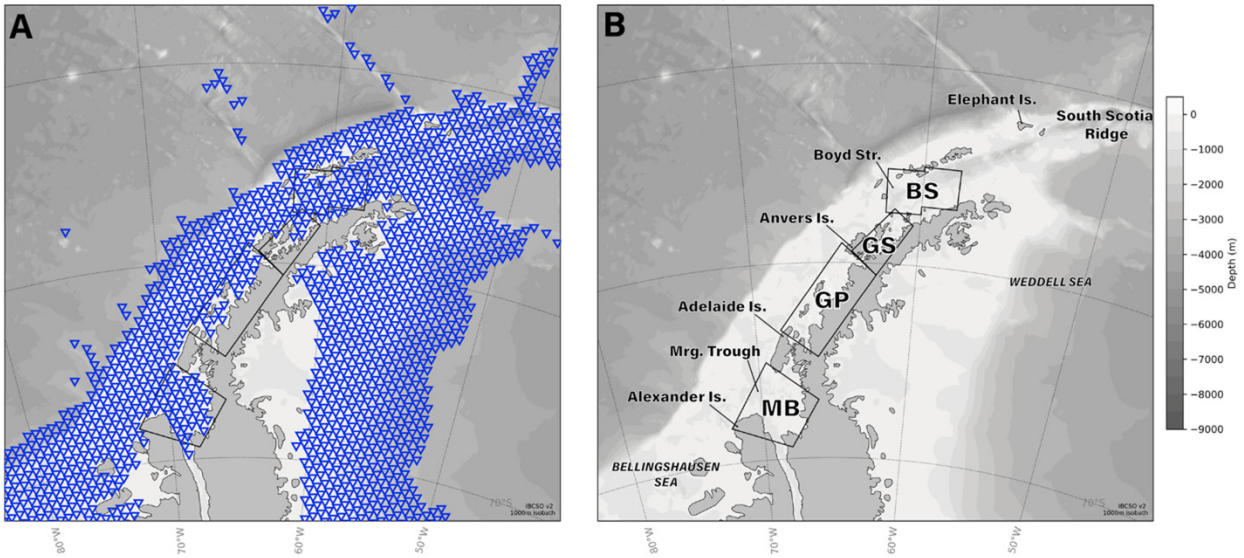

926

927 **Figure 1**: Model Scope and Analysis Reference Region – Panel A identifies the starting

928 locations for all drifters across all scenarios as blue triangles representing all possible

929 spawning locations within the model. Panel B illustrates the four identified nursery grounds:

930 Bransfield Strait [BS-NG], Gerlache Strait [GS-NG], Grandidier Passage [GP-NG], and

931 Marguerite Bay [MB-NG] (see supplementary material for coordinates). Geographic features

932 are labeled (Mrg. Trough - Marguerite Trough).

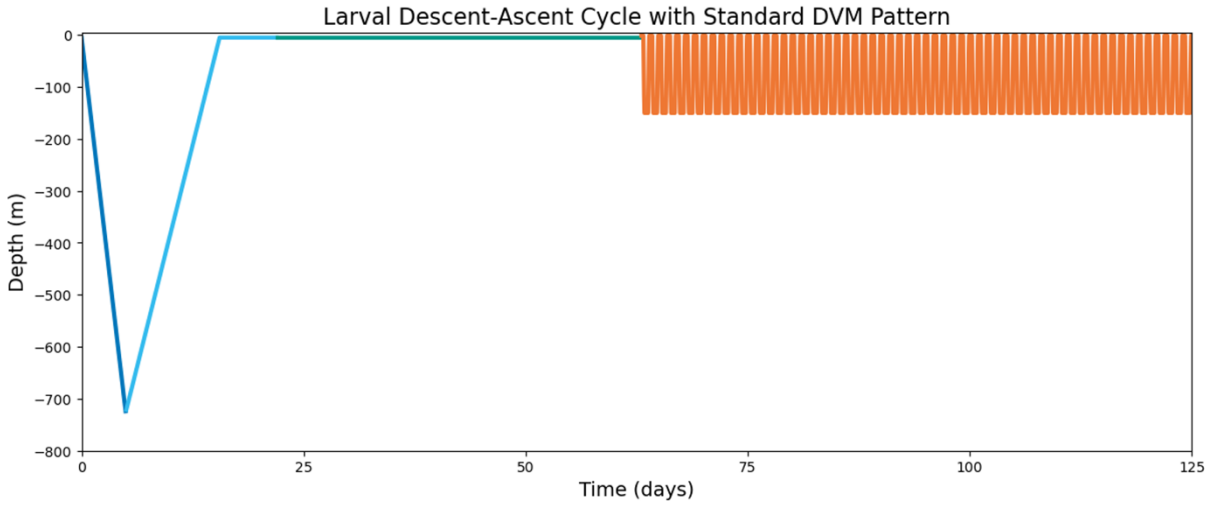

933

Figure 2: Example vertical behavior of a Lagrangian particle representing the early life stages of Antarctic krill, shown here for an embryo with initial diameter of 620 µm. Life stages in the circulation model are defined by elapsed time since embryo release (Hempel, 1979, Ikeda, 1984, Jia et al. 2014, Makarov, 1982). Stages are color coded to illustrate the vertical behavior associated with each phase of development. The schematic depicts the offline-parameterized descent of the embryo in blue, hatching at depth, and subsequent ascent of the larva (nauplii stages: cyan). Early-stage behavior differs between 620 µm and 640 µm embryos (see Table 1), affecting the vertical range and timing of development prior to the onset of diel vertical migration (calyptope stages: green). Diel vertical migration begins after 63 days of development (furcilia stages: orange).

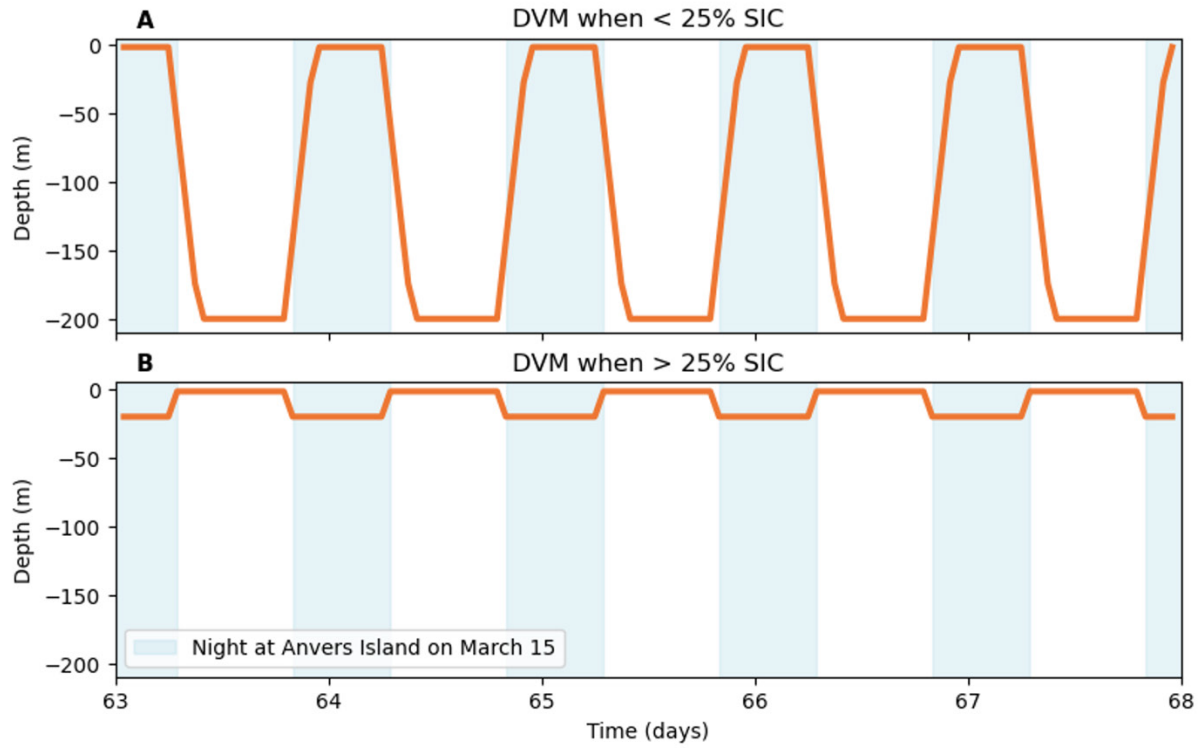

945 **Figure 3**. DVM behavior applied to particles beginning on day 63, once larvae reach the
946 furcilia stage. Panels A and B depict a cross-sectional example of vertical position at Anvers
947 Island, showing differing behavior based on local sea ice concentration. Panel A shows
948 standard DVM in open water (<25% SIC), where particles descend during daylight and
949 ascend at night. Panel B shows reversed DVM under sea ice (>25% SIC), with nighttime
950 descent and daytime ascent.
951

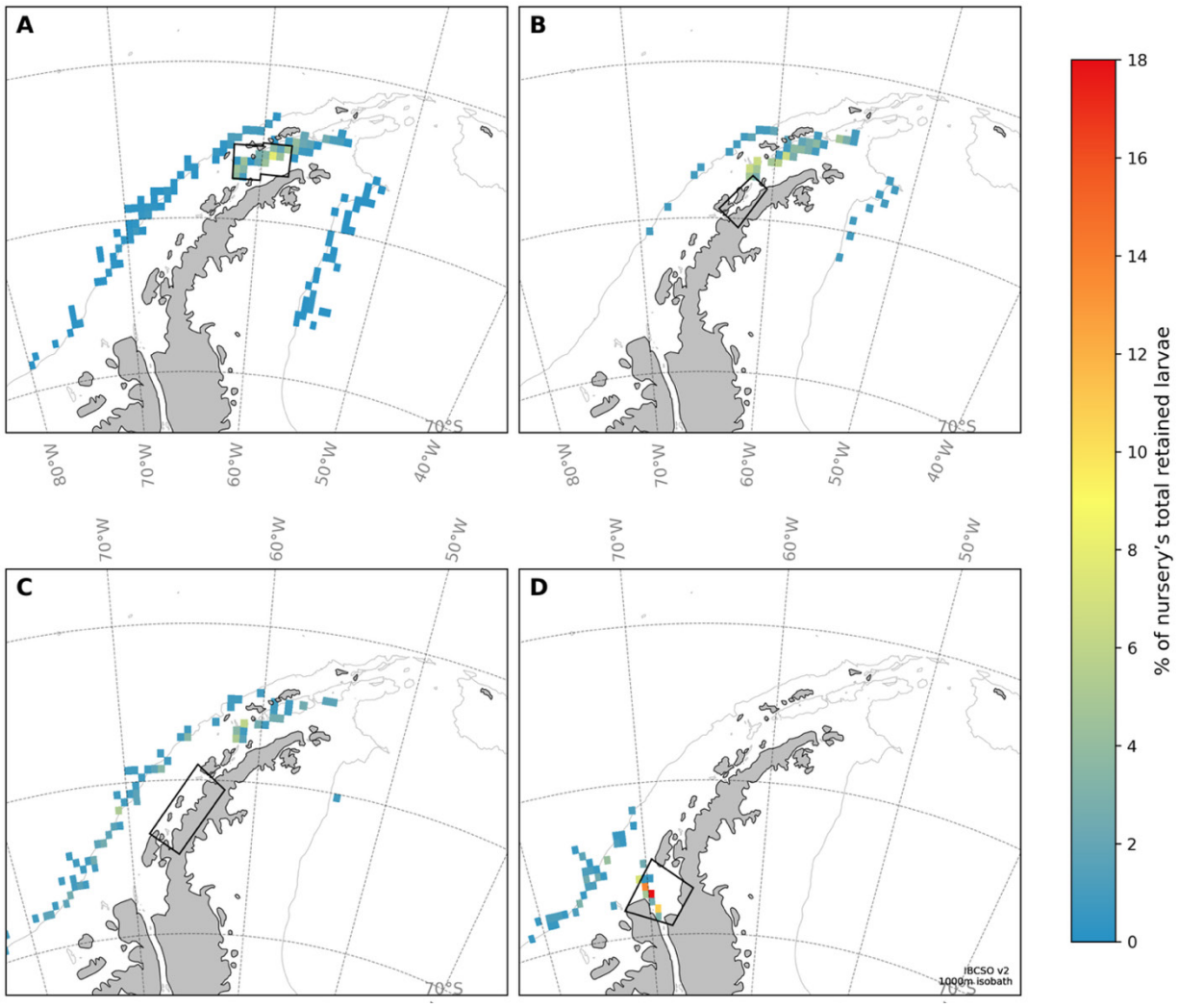

952

953 **Figure 4**: Composite maps of spawning locations of larval krill (620 µm initial embryo size)
954 retained in each nursery ground, aggregated across 2016–2018. Each panel shows the relative
955 spatial distribution of particle release locations that led to successful retention in the
956 respective target nursery, expressed as a percentage of that nursery's total retained larvae.
957 The color scale is shared across panels to enable direct comparison of origin concentration.
958 Total particle counts per nursery (N) are listed in Table 2.

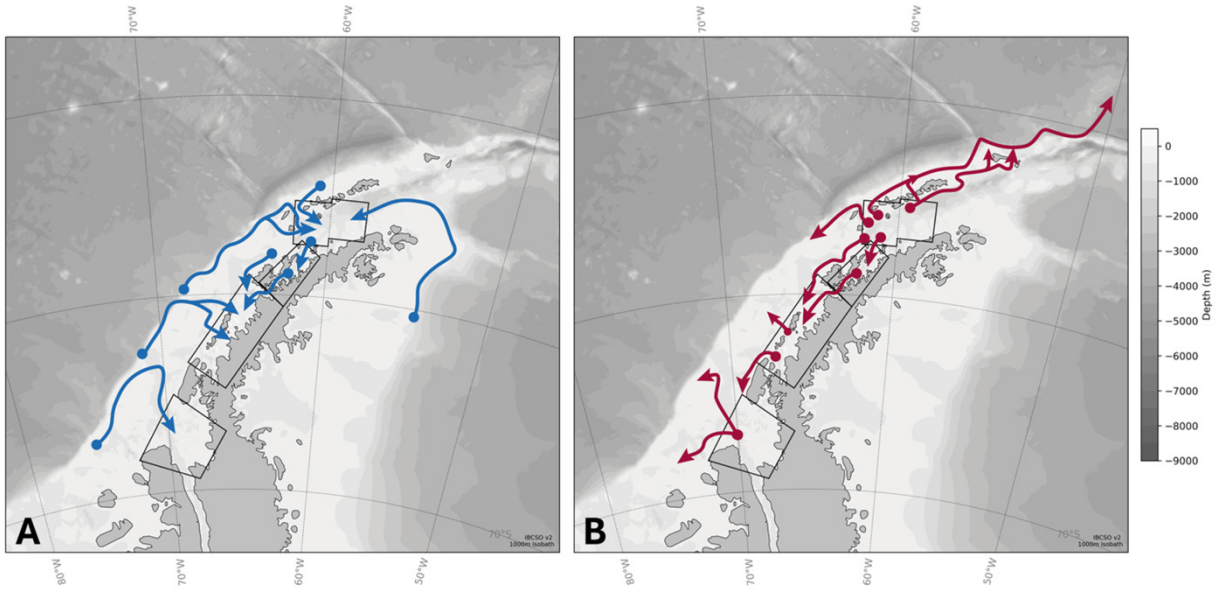

959

960 **Figure 5**: Panels A and B provide a summarization of the trajectories of larvae (620 um
961 embryos) into and out of all nursery grounds (NGs). Panel A summarizes the primary
962 trajectories that advected larvae into NGs while Panel B summarizes the primary trajectories
963 larvae took after exiting an NG.

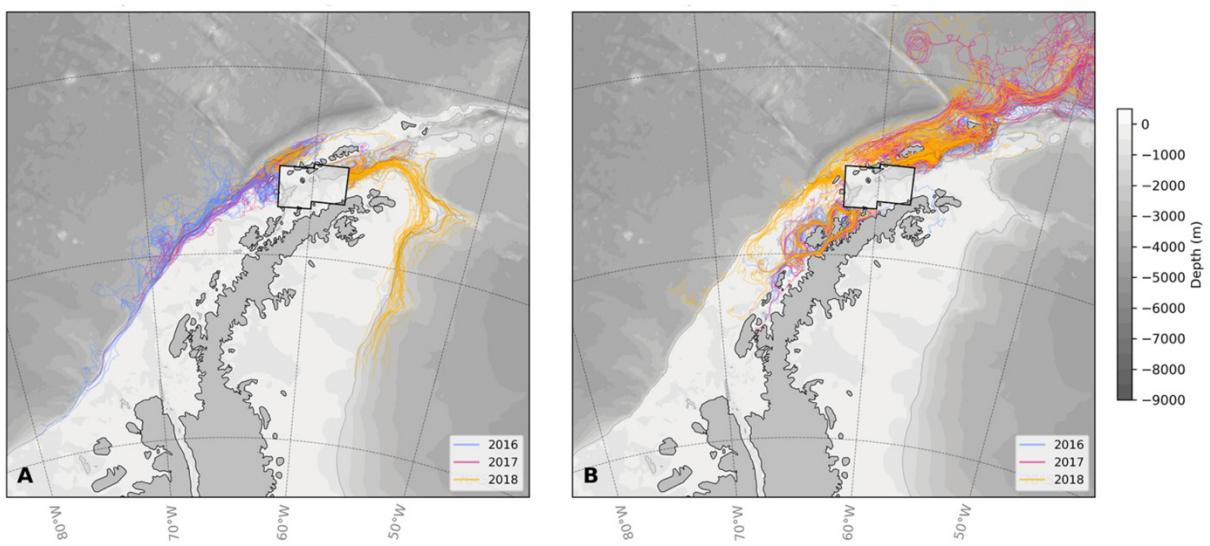

964

965 **Figure 6**: Larval krill trajectories for the Bransfield Strait nursery ground (BS-NG) across

966 three consecutive summers (2016–2019). Panel A shows particle trajectories into BS-NG for

967 larvae not spawned locally. panel B shows trajectories of particles after exiting from BS-NG.

968 Pathways are colored by simulation start year: 2016 (blue), 2017 (magenta), and 2018 (gold).

969 Background shading represents seafloor bathymetry (IBCSO v2).

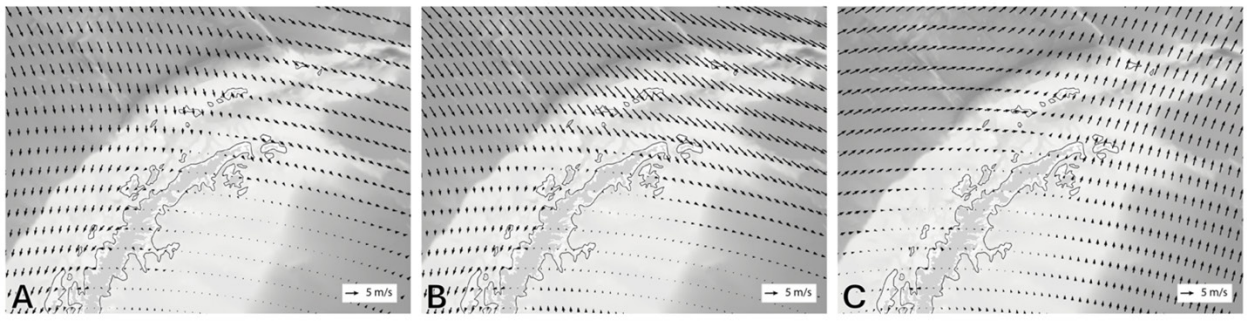

970

971 **Figure 7:** Variability in local near surface (10 m) winds for the month of February are shown

972 for each year: A) February 2017, B) February 2018, C), February 2019. Based onERA5

973 reanalysis data used to force the ocean circulation model. Size of arrows represents wind

974 speed (see scale arrows on each panel).

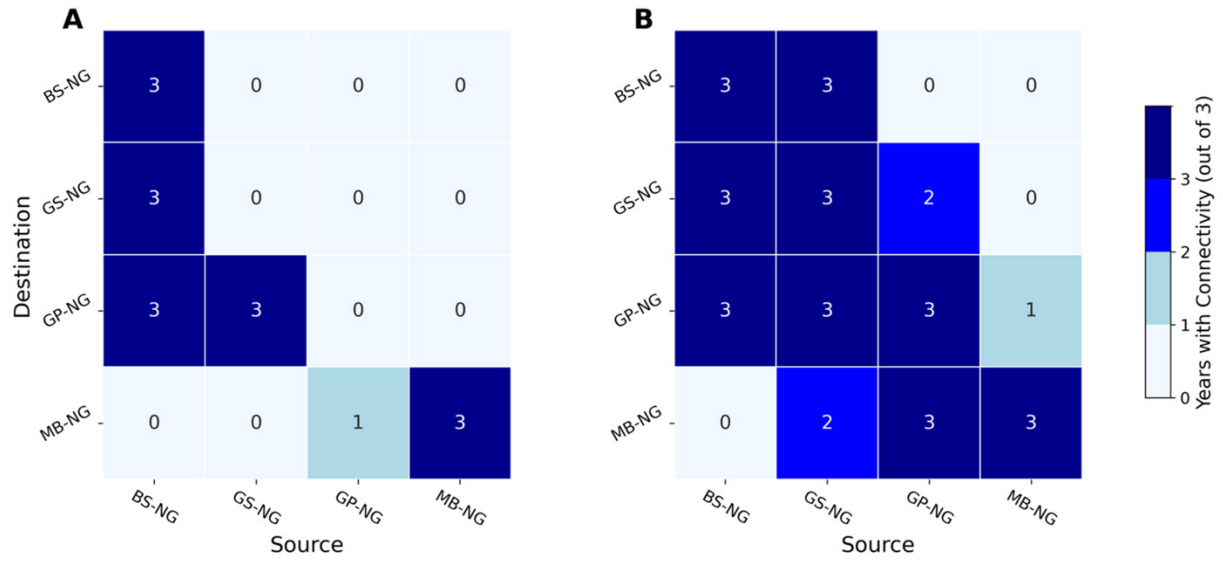

975

976 **Figure 8:** Connectivity matrices of larvae retained by nursery grounds across simulations for
977 (A) 620 µm embryos and (B) 640 µm embryos. Each heatmap shows the number of distinct
978 simulation years (out of 3) in which embryos were spawned in a nursery (source region:
979 columns), before being retained for at least 21 days in the destination NG (rows). Diagonal
980 elements represent self-retention (within the same region), while off-diagonal elements
981 indicate inter-regional connectivity.

982

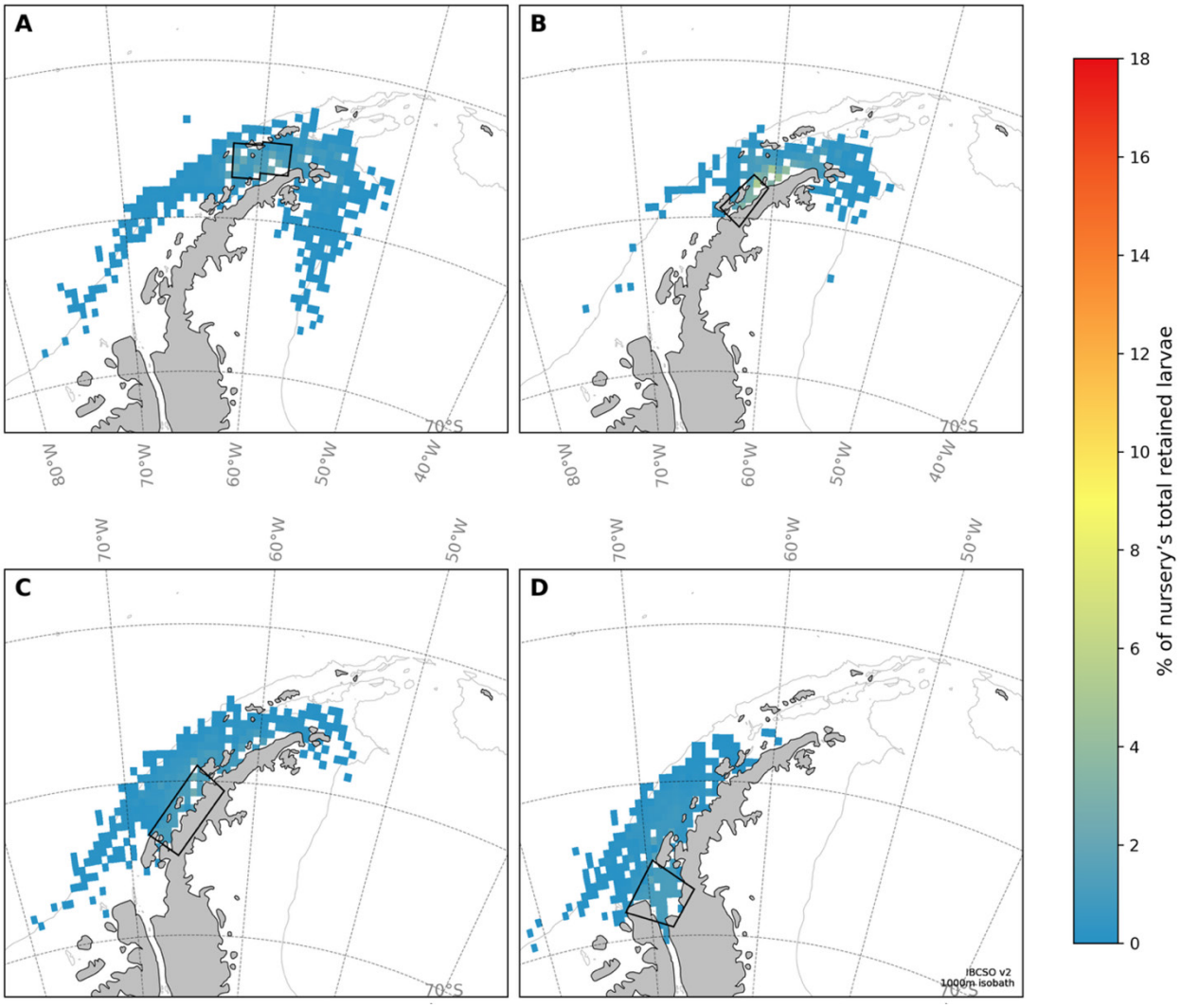

Figure 9. Composite spawning origin maps for larval krill (640 µm initial embryo size) retained in each nursery ground, aggregated across 2016–2018. Each panel shows the relative spatial distribution of particle release locations that led to successful retention in the respective target nursery, expressed as a percentage of that nursery's total retained larvae. Color indicates the fraction of all contributing particles for that nursery that originated in each spatial bin. Values are unitless and reflect relative contributions, not physical densities

990 or temporally resolved information. The color scale is shared across panels to enable direct
991 comparison of origin concentration. Total particle counts per nursery are listed in Table 2.
992

Table 1. Model parameters calculated from the offline descent-ascent model of Hofmann et al. (1992) and the corresponding values used in the online drifter simulations. Parameters were calculated for three locations and for five months (N = 15) for embryos with initial diameters of 620 µm and 640 µm. The parameters include the mean sinking rate of the embryos, their period of descent (*hatching time for 620 µm embryos), mean ascent rate (representing larval swimming for 620 µm embryos and buoyant ascent for 640 µm embryos), and development time to furcilia I (F1). Variability in offline parameters is reported as the mean ± standard deviation. Circulation model inputs represent generalized values applied across all drifters to simulate the descent–ascent cycle and the onset of diel vertical migration (DVM). The circulation model hatching depth was not explicitly parameterized.

Range of Tested Parameters	**620 µm**	**640 µm**
Mean descent rate (m day^{-1})	132.7 ± 1.6	82.1 ± 7.0
Period of descent* (hours)	127.5 ± 15.6	32.2 ± 7.5
Mean ascent rate (m day^{-1})	60.1 ± 6.6	176.2 ± 6.2
Development time to furcilia I stage (days)	65.5 ± 13.9	65.5 ± 13.9
Input parameters for circulation model	**620 µm**	**640 µm**
Descent rate (m day^{-1})	145	80
Period of descent (hours)	120	36
Ascent rate (m day^{-1})	68.2	180
Elapsed time from embryo release until start of DVM (days)	63	63

Table 2 Larval krill use of nursery grounds by initial embryo size (Em Size), averaged across three start years (2016–2018), with annual metrics reported for each nursery ground (NG). Larval influx is the mean number of larvae that entered the NG. Retention duration is shown

1007 as the median retention duration and interquartile range (IQR). Larvae retained is the mean
1008 the number of larvae retained for 21 days or longer. Retention rate is the mean percent of the
1009 larval influx that was retained. The localized spawning percentage shows the mean
1010 proportion of retained larvae inferred to have originated (spawned) locally within the
1011 nursery region. Interannual data are in Supplementary Table 1.

Em Size (μm)	NG	Larval Influx (N)	Median retention duration and IQR (days)	Retained Larvae (N)	Retention Rate %	Localized spawning %
620	BS	316	48 (61)	237	74%	54%
	GS	96	11 (30)	35	37%	NA
	GP	84	20 (33)	39	46%	NA
	MB	75	50 (67)	56	74%	64%
640	BS	1191	41 (61)	833	70%	35 %
	GS	574	25 (42)	299	52%	26%
	GP	1288	44 (80)	895	69%	34%
	MB	1171	58 (71)	960	82%	34%

1012
1013
1014